JRC Scientific and Technical Reports

Fracture Tests to Study the Behaviour of Simulated Sub-Surface Flaws in a Reactor Pressure Vessel Steel

a continuation of the NESC-IV project

N. Taylor [1], P. Minnebo [1], E. Paffumi [1], J. Palyza [2], V. Pistora [2]

[1] Institute for Energy, Petten-Ispra; [2] Nuclear Research Institute, Rez

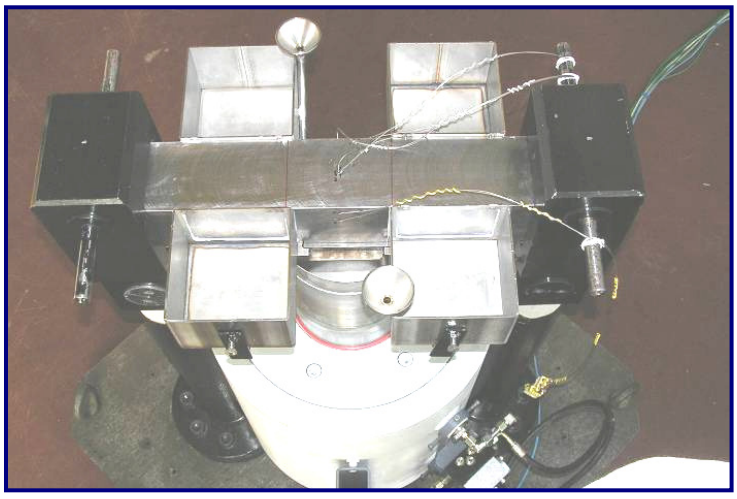

EUR 23970 EN - 2009

JRC EUROPEAN COMMISSION

Institute for Energy

The Institute for Energy provides scientific and technical support for the conception, development, implementation and monitoring of community policies related to energy. Special emphasis is given to the security of energy supply and to sustainable and safe energy production.

European Commission
Joint Research Centre
Institute for Energy

Contact information

N. Taylor

Address: Via E. Fermi 1 - 21027 Ispra (VA) - Italy
E-mail: nigel.taylor@ec.europa.eu
Tel.: +39 033278 3604
http://www.jrc.ec.europa.eu

JRC 52752

EUR 23970 EN

Luxembourg: Office for Official Publications of the European Communities

Printed in The Netherlands

EXECUTIVE SUMMARY

The NESC-IV project (2000 - 2005) addressed the transferability of fracture toughness data from laboratory specimens to applications that assess the integrity of reactor pressure vessels. This project included a series of uniaxial bend tests on large beams with a simulated shallow, sub-surface flaw. The results of these experiments pointed towards a significant constraint-loss effect in the ductile-to-brittle transition temperature range of the used steel, but in view of the inherent scatter in fracture toughness of low alloy steels in the given regime, further testing was recommended.

Therefore the scope of present project was to perform a set of six additional tests with nominally identical test piece geometry, material and loading arrangements, so as to obtain a statistically more relevant data set. The Institute for Energy contracted the Nuclear Research Institute in Rez to perform these experiments. Following the successful execution of the tests, a preliminary fracture mechanics analysis was made to compare estimates of the stress intensity values at failure with the material's Master Curve. The results confirmed the constraint-loss effect, which had been observed in the previous NESC-IV test series. Moreover it was found that some aspects needed further attention, such as detailed finite element modelling of the experimental arrangements and accurate characterization of the test material's fracture toughness. The latter should also consider material inhomogeneity issues.

CONTENTS

1 INTRODUCTION

For light water reactors the integrity of the reactor pressure vessel (RPV) has to be demonstrated for severe overcooling transients, considering also that crack-like flaws could be present in the vessel wall [1]. For safety assessment purposes postulated flaws are generally assumed to be surface breaking, located on the inner clad surface and of semi-elliptical form. Studies on actual defect distributions indicate that RPV flaws, if present at all, are more likely to be sub-surface [2]. This has prompted a series of studies aimed at optimising the fracture mechanics procedures for evaluating brittle fracture initiation at such defects. These procedures need however to be properly validated against experimental data. A series of projects by the Network for Evaluating Structural Components (NESC) seeks to address this issue. Specifically, this report provides details of a set of large scale bend experiments on test beams containing a simulated sub-clad flaw. This is a continuation of work performed in the NESC-IV project [3], which demonstrated the feasibility of conducting such tests on clad and unclad test pieces. To reinforce the statistical validity of the NESC-IV work, the Institute for Energy (IE) contracted the Nuclear Research Institute (NRI) in Rez to perform a further six tests on the clad test piece design. These experiments have been successfully completed. The following sections provide a summary of the experimental methodology, the results and the preliminary analysis. Further details of this work are given in the NRI test report [4].

2 TEST PROGRAMME

2.1 BACKGROUND AND SCOPE

The NESC-IV project demonstrated the feasibility of performing tests on large beams with a simulated sub-surface flaw in the form of a long slot (Figure 1). Oak Ridge National Laboratory (ORNL) carried out four tests in all, two on test pieces with a clad layer and two on beams without cladding. The results pointed towards a significant constraint-loss effect in the ductile-to-brittle transition temperature range of the used RPV steel, but in view of the inherent scatter in fracture toughness of low alloy steels in the given regime, further testing was recommended. Therefore the scope of the present series was to perform a set of six tests on clad specimens using nominally identical test piece geometry, material and loading arrangements (Figure 2), so as to obtain a statistically relevant data set.

The most critical test parameter is temperature, which should be sufficiently low to produce brittle fracture with contained yielding at the crack tip, but above the lower shelf. Using the NESC-IV results as a guide, a nominal test temperature of -95 ^{o}C was selected.

The results of the programme serve to evaluate the usefulness of fracture mechanics assessment methods, in particular the Master Curve approach, as well as advanced concepts designed to exploit the beneficial effect of constraint loss.

2.2 MATERIAL

Materials for the test sections were machined from a segment of the PVRUF vessel (USA), which was never put in service. It was fabricated in A533 B low alloy steel with a single-layer stainless steel strip-clad overlay (100 mm wide and ~5 mm thick) on the inner surface. The

shell had a nominal inner radius of 2210 mm and a thickness of 232 mm (including the clad overlay). The longitudinal submerged-arc welds, which were present in the RPV, used A533 B Class 1 filler metal and had a double-J configuration with the weld root located at approximately 1/3 of the wall thickness, starting from the inner surface.

The mechanical and fracture properties of the A533 B plate, the longitudinal weld, the clad overlay, the clad/plate heat affected zone (HAZ) and the clad/weld HAZ were investigated in the NESC-IV project. A full description of the results is given in the NESC-IV final report [3]; the fracture properties and associated Master Curve analysis have also been published separately [5].

2.3 SPECIMEN DESIGN AND FABRICATION

Figure 3 shows an engineering drawing of the test specimens. Each beam was made up of three sections. Only the middle part of the specimen, referred to as the insert, was clad. The locations of the inserts in the PVRUF shell are shown in Figure 4.

The fabrication was coordinated by IE. The extension arms were machined from the same PVRUF material, but taken from the outer part of the vessel wall. This optimised the use of the inner clad surface material, which is of primary interest for fracture assessment investigations. The arms were electron beam welded to the insert to ensure that the crack location was not unduly heated. Figure 5 shows for example the central section of specimen no. 1. PTR GmbH performed the electron beam welding, but regrettably the quality was not always optimal. Difficulties were reported in starting the weld cleanly and in several cases the beam "tripped" during welding and had to be restarted. As a result some grinding and weld repairs were carried out before testing in order to eliminate weld defects which could lead to fracture of the extension arms rather than at the embedded flaw location. Further details are available in the fabrication report [6] and the NRI test report [4].

The simulated sub-surface flaws had a nominal height of 21.3 mm. The upper tip was located approximately 13 mm under the clad surface. For the flaw insertion, a wire electro-discharge machining (EDM) process was used to create a uniform crack-like slot of 0.3 mm width. To allow the wire to pass through the beam a small hole was first drilled; then the EDM machine cut the slot above and below the starter hole. The major advantage of this procedure is that there is no metallurgical alteration of the material between the flaw tip and surface.

Both crack tips were sharpened by fatigue cycling of the specimen at SVUM in the Czech Republic. The fatigue crack growth towards the cladding was about 1.7 mm; in the depth direction it was about 0.2 mm. This represents a slight difference to the situation in the NESC-IV tests, where the lower crack tip was not sharpened. The initial intention had been to use the same conditions as reported for NESC-IV, with $K_{max} < 25$ MPa$\sqrt{m}$. It was however argued that a higher load amplitude, combined with a fairly high R ratio would favour more uniform crack growth compared to low load amplitudes, when local material inhomogeneities or residual stresses can cause local differences in the growth. A higher load amplitude was therefore agreed, namely $K_{max} < 50$ MPa$\sqrt{m}$ and a load ratio $R = 0.2$, to minimise differences in crack closure effects. Examination of the cracks after fracture tests confirmed that the procedure produced very straight crack fronts. These conditions also produced sharpening at the lower notch tip, which has the advantage of removing ambiguity for assessing the probability of brittle fracture initiation at this point, i.e. it can be treated as sharp crack rather

than as a notch. Precise measurements of the actual defect dimensions were performed after the testing and are summarised in Table 1. The nominal values for the test pieces used in the NESC-IV series are included for reference.

Table 1 Test piece dimensions and crack locations (all values in mm).

Specimen	Beam section		Total crack height	Ligament to upper surface	Mean clad thickness		Pre-fatigue crack length	
	Width	Height			Pre-test	Post-test	Shallow tip	Deep tip
1	101.7	102.4	22.00	12.25	6.60	6.38	1.63	0.37
2	101.7	101.7	22.19	12.18	6.20	5.85	1.77	0.41
3	101.7	101.8	22.02	11.93	5.60	5.41	1.63	0.39
4	101.7	102.3	22.26	12.21	6.60	6.15	1.87	0.39
5	101.7	102.2	22.17	12.55	5.40	5.02	1.81	0.37
6	101.7	101.3	22.00	12.04	6.05	6.12	1.66	0.34
Average	101.7	102.0	22.11	12.19	6.08	5.82	1.73	0.38
NESC-IV (nominal)	101.6	101.6	21.3	12.7	5.0	-	1.3	0.0

3 EXPERIMENTAL PROCEDURE

3.1 TEST EQUIPMENT

The experimental set-up is shown in Figure 6. The specimen is located on the central mast, centred by a fastener. The dimensions of the support plate below the test specimen are 114 x 114 mm, which is somewhat larger than in the original NESC-IV test series performed at ORNL (101 x 101 mm). The distance between the loading locations is 610 mm. The load is applied by a central hydraulic cylinder with a total capacity of 2.5 MN, although the maximum allowable force for testing beam specimens on the experimental equipment is 1.3 MN. The test beam is loaded against two edges located symmetrically at 57 mm from the central axis. Thus, in the area of the central part of the specimen, where the defect is located, there is a constant bending moment over the whole length between both supporting edges. The distance between the symmetrical loading locations and the supporting edges is 248 mm; the maximum bending moment is equal to 161 kNm. For safety during testing the equipment is surrounded by a cage to catch any flying parts released from the system.

Since the nominal test temperature was -95 ^{o}C, the test section was cooled by liquid nitrogen (see Figure 7). To calibrate the system, a mock-up was manufactured and instrumented with 8 thermocouples placed in the symmetry plane of the mock-up. Before the calibration test, the mock-up was loaded with about 10 kN to assure contact with the supporting mast. It was then cooled by pouring liquid nitrogen into four vessels attached to the specimen arms and one vessel cooling the top of the central mast. The temperature was reduced to about -140 ^{o}C and then allowed to increase. At about -90 ^{o}C liquid nitrogen was added again to decrease the temperature. This cycle was repeated four times. The resulting temperatures from the thermocouples are shown in Figure 8. The behaviour is similar in all four cycles.

Figure 9 shows details of the second cooling and heating cycle. During the free heating phase the temperature field in the test section is almost equalised. The exception is thermocouple T2, which is influenced by the heat flux from the relatively warm and massive piston, but is

also well away from the crack tip position. It was therefore decided to apply only two cooling cycles for the actual tests and to fracture the specimen in the final stage of the second free heating phase. Thermocouple position T7 (in the drilled hole of the simulated flaw) was selected as reference because of its simple installation and very good agreement with the crack tip temperatures.

3.2 TESTING METHOD

The applied procedure was as follows:

1. Identification of the specimen, identification of loading and fracture parameters, measurement of the initial specimen dimensions.
2. Assembly in the test equipment, pre-loading to approximately 10 kN, installation of measuring devices.
3. Start of cooling by liquid nitrogen, 2 cycles of cooling to approximately 40 ^{o}C lower than the prescribed testing temperature followed by free heating up to the required temperature. Continuous logging of the temperature by 2 thermocouples. The fracture test is started at the end of the second cycle when temperature is 5 ^{o}C below the prescribed testing temperature.
4. To obtain high-speed video pictures of the crack tips, the flank of the specimen is de-iced by spraying the surface with a small amount of ethanol.
5. Fracture test is realised by loading with a constant displacement rate (piston velocity) of 2 mm/min up to specimen fracture. All measured parameters are continuously recorded. (The fracture phase of the tests usually lasted about 2 to 3 minutes)
6. After dismounting the specimens, the fracture surfaces are treated to conserve them against corrosion.
7. A database of the raw measured parameters is created on CD.

3.3 MEASUREMENTS

During the test, the following parameters were measured and recorded in real time:

- F [kN], the total applied force in the central mast;
- LLD [mm], the Load Line Displacement from the movement of the piston rod with respect to the body of the hydraulic cylinder;
- CMOD [mm], Crack Mouth Opening Displacement using a clip gauge attached to the side of the specimen on the fabricated slot; the device was calibrated for a range of up to 2.5 mm (accuracy ± 0.3 %);
- T [^{o}C] specimen temperature measured by 2 thermocouples on both sides of the drilled hole (in the centre of specimen height).

All transducers were calibrated together with the respective measuring apparatus. Calibration certificates are available as part of the NRI report [4]. The following sections provide further details of the LLD and CMOD measurements, as well as the crack-tip video imaging recordings.

3.3.1 CMOD

Crack Mouth Opening Displacement (CMOD) measurements were made using clip gauges attached at either side of the specimen. Each CMOD gauge was calibrated separately using a Mitutoyo position transducer. One arm of the measuring device was fixed to the specimen by a screw, while the other arm was ended by an edge touching the specimen on the opposite crack face. To enable this touching, a small notch was machined on the flank surface of the specimen. The centre of the notch, i.e. the position where CMOD is measured, was located 21 mm below the specimen top, i.e. 8 mm above the centre of the drilled hole, about 2 mm above the crack centre. For specimen no. 1 and 5 measurements were performed on both specimen flanks; for the other specimens measurements were made at one side only to leave the other side free for the video recording of the crack tip. Figure 10 shows the device for CMOD measurement mounted on the flank of a specimen.

3.3.2 LLD Compliance Correction

The Load Line Displacement (LLD) was measured during the tests from the extension of the hydraulic ram piston relative to the piston body. This however needed to be compensated for machine compliance to convert it to the value on a test specimen. As a basis for this, a special series of compliance measurements was performed using a very thick mock-up specimen. These measurements were carried out for several load levels up to 1 MN. Details are given in the NRI test report [4]. The resulting correction ΔLLD is shown as a function of applied load in Figure 11. The 5th order polynomial fit is as follows:

$$\Delta LLD = 7.429x10^{-15}.F^5 - 2.040x10^{-11}.F^4 + 2.071x10^{-8}.F^3 - 9.601x10^{-6}.F^2 + 3.377x10^{-3}.F + 3.151x10^{-2}$$

where ΔLLD is in mm and F is in kN. This amount is subtracted from the measured LLD to give a "true" value.

3.3.3 High-Speed Video Imaging of Fracture Initiation

At the initiative of NRI, several tests were recorded with a high-speed video camera in an effort to distinguish which crack tip (shallow or deep) initiated first. This is important since it influences the interpretation of the test result regarding the effect of constraint; furthermore the issue was not resolved in the first round of NESC IV beam tests. Two cameras made by Fastec Imaging Corporation were used:

1. TroubleShooter, Model TS1000ME (with recording frequency of 1,000 Hz);
2. TroubleShooter HR, Model HR16000SM (with recording frequency of 16,000 Hz).

Since cleavage fracture of low alloy steel is very fast, with a velocity of crack propagation of about 1,000 m/s, a crack can propagate through the whole beam during one or two snaps with the 16,000 Hz frequency camera, and the possibility of distinguishing the initiating point is at the limit of its capabilities. The faster camera had, of course, smaller graphical resolution (32x1280 pixels) than the slower one (480x640 pixels). Due to this the interpretation of resulting images was difficult. To assist the interpretation, software provided with the camera was used to make a digital check of the differences between consecutive images i.e. to detect if a crack was starting to run at either the deep or shallow tip.

4 RESULTS

In total six specimens were tested. Specimen no. 1 was successfully tested at -95 ^{o}C in September 2006 as a pilot test. On the basis of this result, also the other specimens were fatigue sharpened at SVUM and the main testing schedule started in November 2006. The first four tests produced fracture at loads at the upper end of the expected range and as a result for the remaining tests it was decided to lower the temperature by approximately 10^{o}C. Specimen no. 6, which was tested at -108 ^{o}C, failed prematurely in one of the electron beam welds connecting the extension arms with the insert (Figure 12). A repair weld was performed and the specimen was successfully retested in May 2007 to produce a fracture at the crack. For each test data of temperature at thermocouple no 7, of the force, LLD and CMOD were stored in an Excel file, which is available from the JRC. The values of the main parameters at fracture are summarised in Table 2. Concerning the CMOD measurements, in the first two test performed (numbers 1 and 5), two clip gauges were used, one on either side of the specimen. These produced almost identical readings and for the remaining tests only 1 clip gauge was used to allow better access for the video camera to the crack tip on one side. In the test on specimen 3, the CMOD readings were unfortunately lost shortly after the start of loading. All specimens failed directly after initiation of fracture, with the crack propagating downwards and then bifurcating at a position about 1/3 of specimen height (from its bottom). Further propagation occurred to some extent in horizontal direction to both sides. Figure 13 shows an example of such behaviour.

Table 2 Results of the fracture tests

Spec. no.	Test temp.	Force at fracture	LLD at fracture	CMOD at fracture	Comment
	[ºC]	[kN]	[mm]	[mm]	
1	-95	995	3.83	0.327 (0.332)	2 CMOD measurements
2	-110	783	2.45	0.129	Repaired weld
3	-94	1057	4.47	-	CMOD measurement failure
4	-94	1013	3.86	0.351	Repaired weld
5	-94	1018	3.65	0.300 (0.302)	2 CMOD measurements
6	*-108*	*775*	*2.37*	*0.118*	*Specimen failed prematurely in weld; invalid result*
6*	-108.5	986.5	4.93	0.298	Tested after rewelding of extension arm

The instrument output is summarized in graphical form in the following figures.

Figure 14 shows the temperature variation for thermocouples 1 (middle of upper clad surface) and 8 (specimen flank at deep crack tip) for the period of the fracture test and confirms the good degree of uniformity of the temperature field.

Force vs. LLD curves for all 6 tests are shown in Figure 15, both as-measured values and values corrected for machine compliance. To avoid differences caused by the settling of individual specimens at the loading points (influencing the initial part of the force vs. LLD diagrams), another correction was applied: the linear parts of the force vs. LLD curves (corrected to machine compliance) were linearly extrapolated from the region 300 - 500 kN to zero LLD. Then the data were shifted so as the start of this linear extrapolation is at the origin. The resulting curves are shown in Figure 16.

Figure 17 shows the applied load as a function of CMOD. The measured values were shifted to start at 0 for zero loading. For specimen nos. 1 and 5, where two CMOD measurement devices were installed on either side of the specimen, both curves are presented. The predicted force vs. CMOD curve from a linear elastic finite element model (with crack included in the mesh) is included in Figure 17. For the initial linear part of the test, the agreement is very good, confirming the reliability of the measurements. In specimen no. 3 the CMOD device failed during the test; the triangle in Figure 17 indicates the limit of the valid measurements. Nevertheless, this specimen can be analysed with fracture mechanics, as the force and LLD data were recorded up to fracture and good agreement of force vs. LLD as well as force vs. CMOD curves for all 6 specimens means that a simple cross-correlation can be used to infer the CMOD at fracture.

Figure 18 compares the moment (M) vs. CMOD data with the corresponding results from the Clad 4.1 test performed at - 95^{o}C in the original NESC-IV test series. Although the testing set-up is nominally the same, the present series of NRI tests show a stiffer behaviour, i.e. a greater moment needs to be applied to produce a given level of CMOD. The difference is noticeable from the start of loading, suggesting that a systemic effect is present in the test set up.

As mentioned above, the use of the high speed video recording of the crack tips was a special innovative feature of these tests. The recordings with the 1,000 Hz camera showed that the fracture event occurred between two consecutive frames (see Figure 19, for example), and therefore no information can be derived on the location of initiation (shallow or deep tip). The 16,000 Hz camera was used in only three tests (nos. 2, 3 and 5). For specimen no. 2, fracture happened during one snap, even for this very high speed camera (Figure 20). Some very minor movement at the tips is seen before the fracture. For specimen no. 3 the fracture of the specimen appears again to have happened between frames (Figure 21). For specimen no. 5 the records from the 16,000 Hz camera are presented in Figure 22. The middle part of the crack is partially covered by the CMOD gauge in this case. It appears that fracture initiated at the deep crack tip, one frame (1/16000 secs) earlier than the shallow crack tip. This is reinforced by the images showing the differences between successive frames, which are included in Figure 22.

5 "QUICK LOOK" ANALYSIS

A preliminary fracture mechanics analysis has been performed to provide a "quick-look" assessment of the results. This consists in plotting the estimated stress intensity values at fracture (K_{Jc}) from each of the tests and for both the shallow and deep crack tips together with the representative Master Curve for the PVRUF material.

The sub-surface crack configuration and the presence of the clad layer mean that standard K or J solutions are not strictly applicable. It had been hoped to directly use the solutions developed in the NESC-IV project to provide K_J estimates. However as noted above, the beams in the present series show slightly greater stiffness than the corresponding ORNL data, so ideally new cracked-body FE calculations should be performed with the exact geometry of the beams and the NRI test rig. For the purpose of this quick look analysis we have simply assumed that the CMOD - K_J relationships established in the NESC-IV tests (Figure 23) can be used to provide an estimate of K_J at fracture for the NRI specimens (both shallow and deep crack tips). These K_J estimates were first size-corrected to the standard Master Curve crack length of 25 mm using the relation:

$$K_{Jc} = 20 + \left(K_{Jc(\exp)} - 20\right)\left[\frac{B_{\exp}}{25}\right]^{1/4}$$

where B_{exp} = 102 mm. Table 3 summarises the values obtained, together with the NESC-IV results.

Table 3 Summary of the results of fracture tests on beam specimens with embedded flaws

Test	Clad / unclad	Test temp.	CMOD at fracture	K_J at fracture		K_J (crack length corrected)	
				shallow	deep	shallow	deep
		°C	mm	MPa.√m	MPa.√m	MPa.√m	MPa.√m
NESC-IV							
4-1-1	unclad	-128.1	0.056	48	32	60	37
4-1-2	unclad	-95.4	0.378	219	164	303	224
4-2-1	clad	-93.2	0.262	147	108	200	145
4-2-2	clad	-77.2	0.729	220	165	304	226
NRI							
No. 1	clad	-96	0.330	190	127	261	172
No. 2	clad	-111	0.129	89	56	118	72
No. 3	clad	-95	0.414	232	157	321	214
No. 4	clad	-95	0.351	200	135	276	183
No. 5	clad	-95	0.301	175	117	240	158
No. 6	clad	-108	0.298	174	116	238	156

N.B. the K_J values for the NRI tests are based on the NESC-IV CMOD vs. K_J correlation.

In this study the fracture resistance of the material as a function of temperature is represented by the Master Curve, which is indexed with the T_0 parameter. As described in the NESC-IV documentation [3], the situation is complicated by the fact that the fracture properties were found to vary between the different plates used to fabricate the PVRUF vessel. For the present

analysis a T_0 value of 100°C is taken, corresponding to high-constraint data for the so-called "Plate 100" (obtained from 25 mm thick C(T) specimens). Fracture tests on material taken from the sampling location for the test beams are underway to provide a definitive reference point.

The analysis must also take account of constraint loss effects which can suppress fracture initiation by allowing more crack tip plastic flow. In NESC-IV the situation for this specimen design was summarised as follows: without considering constraint, fracture is always more likely for the shallow than the deep tip, since the K value is higher at that point. If constraint loss is considered, three regimes can be identified. Well below the T_o temperature, failure is predicted at the shallow tip first; well above T_o, fracture is predicted at the deep tip first. In the intermediate range, the failure probability curves for the shallow and deep tips cross at a certain load level. Up to that point, fracture initiation is predicted at the shallow tip; above it, initiation is more likely at the deep tip (due to the constraint loss at the shallow tip at higher loads).

Figure 24 and 25 show the K_J data for the deep tip and the shallow tip, respectively, together with the NESC-IV data and the T_0 = -100 °C Master Curve. For the deep tip, the values from the tests performed around -95 °C lie above the Master Curve P_f = 95% upper bounding line. For the same group of tests, the shallow tip K_J values are substantially above the Master Curve. The video camera evidence for specimen no. 5, which was in this group, suggests that the fast fracture event initiated at the deep tip. Hence the hypothesis is that at this temperature level the constraint loss effect at the shallow tip suppresses fracture initiation (even if though the K_J level is higher). Instead the fracture starts at the deep tip, and the fact that the K_J lie slightly above the Master Curve suggests that even this point may experience some constraint loss effect.

The remaining tests (no 6 and no.2) were performed at the lower temperatures of -108 and -110 °C respectively. In neither case were the video images successful in providing clues as to which tip started the fracture. For specimen no. 6 the K_J values for both the shallow and deep points lie above the Master Curve suggesting behaviour similar to the group tested at -95 °C. On the other hand for specimen no. 2 both K_J values lie within the Master Curve bounds, so at this point no conclusive statement can be made about the location for the start of the fracture event.

6 CONCLUSIONS

- A series of six uniaxial bend tests were successfully completed on large-scale beam test pieces containing a simulated sub-surface flaw. Full details of the test procedure and results are now available.
- For three tests NRI took the innovative step of using a high-speed video camera (16,000 Hz) to monitor the two crack tips during loading. In one case the images indicate with some certainty that fracture initiated from the deep crack tip, while for the other tests it is not possible to distinguish which crack tip initiated first.
- A preliminary fracture mechanics analysis has been made to compare estimates of K_{Jc} with the Master Curve for this material; the results confirm a significant constraint loss effect, in line with that observed in the previous NESC-IV test series.

- JRC is now performing further work on several items: to check the fracture surfaces for initiation points, to resolve differences in the moment vs. CMOD curves between the 1st (ORNL) and 2nd (NRI) test series, to determine K_J values for the exact test piece geometry and loading arrangement used in the 2nd series and to verify the Master Curve T_0 value for the specific PVRUF plate from which the beams were machined. The results will be presented in due course[1].

7 ACKNOWLEDGEMENT

This research project would not have been successful without the competence and enthusiasm of the technical staff involved both at IE and NRI. This particularly applies to the fabrication of the test pieces and the performance of the experiments.

8 REFERENCES

[1] "Assessment and Management of Ageing of Major Nuclear Power Plant Components Important to Safety: PWR Pressure Vessels", IAEA-TECDOC-1120, International Atomic Energy Agency, 1999

[2] F.A. Simonen, G.J. Schuster, S.R. Doctor, T.L. Dickson, "Distributions of Fabrication Flaws in Reactor Pressure Vessels for Structural Integrity Evaluations", ASME PVP, vol. 433-2, p. 133-143, American Society of Mechanical Engineers, 2002

[3] N. Taylor et al, "An Investigation of the Transferability of Master Curve Technology to shallow Flaws in reactor Pressure Vessel Applications", Final Report NESC-IV Project, EUR 21846 EN, European Commission, 2005

[4] J. Palyza, V. Pistora, "Report on NESC-IV Large Scale Tests", Report DITI 301/397, Nuclear Research Institute Rez plc, 2006

[5] N. Taylor et al, "Use of Master Curve Technology for Assessing Shallow Flaws in a Reactor Pressure Vessel Material", Journal of Pressure Vessel Technology, vol. 130, issue 3, 031407, 2008

[6] J. Mendes et al, "Fabrication Report for the Second Series of Embedded Flaw Beams", NESCDOC (04)08, European Commission, 2005 (*available on request from IE*)

[1] ASME Pressure Vessels and Piping Conference, July 2009

9 FIGURES

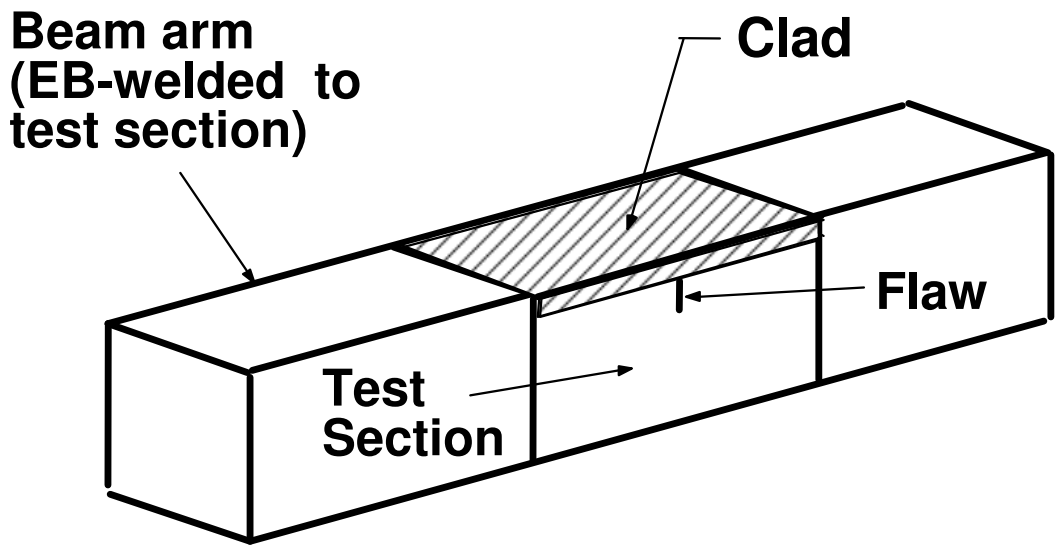

Figure 1 Clad beam test piece developed in the NESC-IV project.

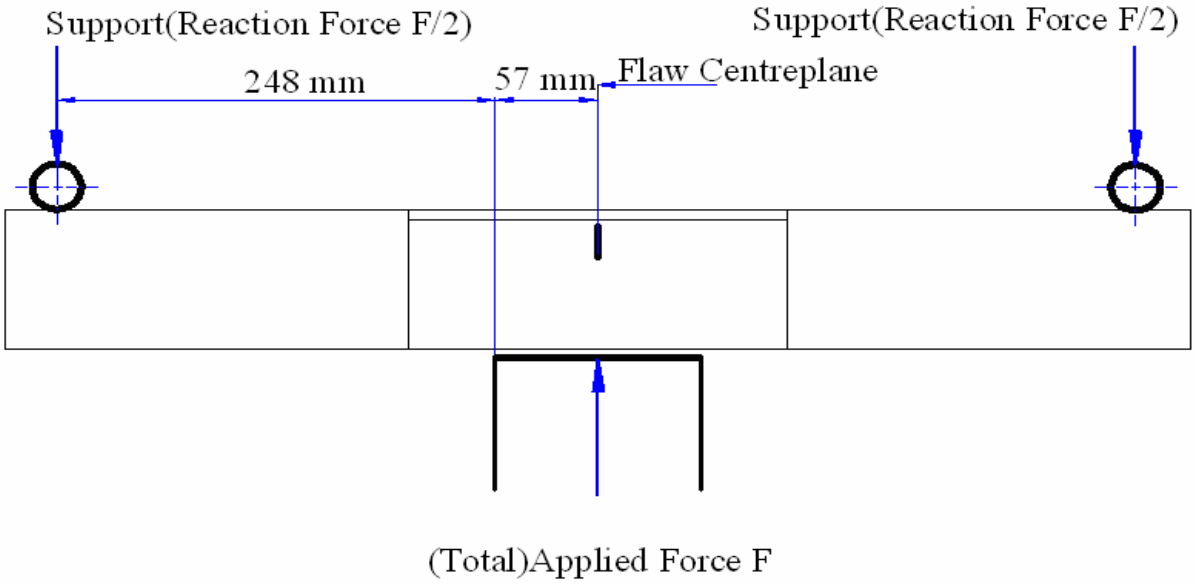

Figure 2 Loading arrangement for the NRI tests.

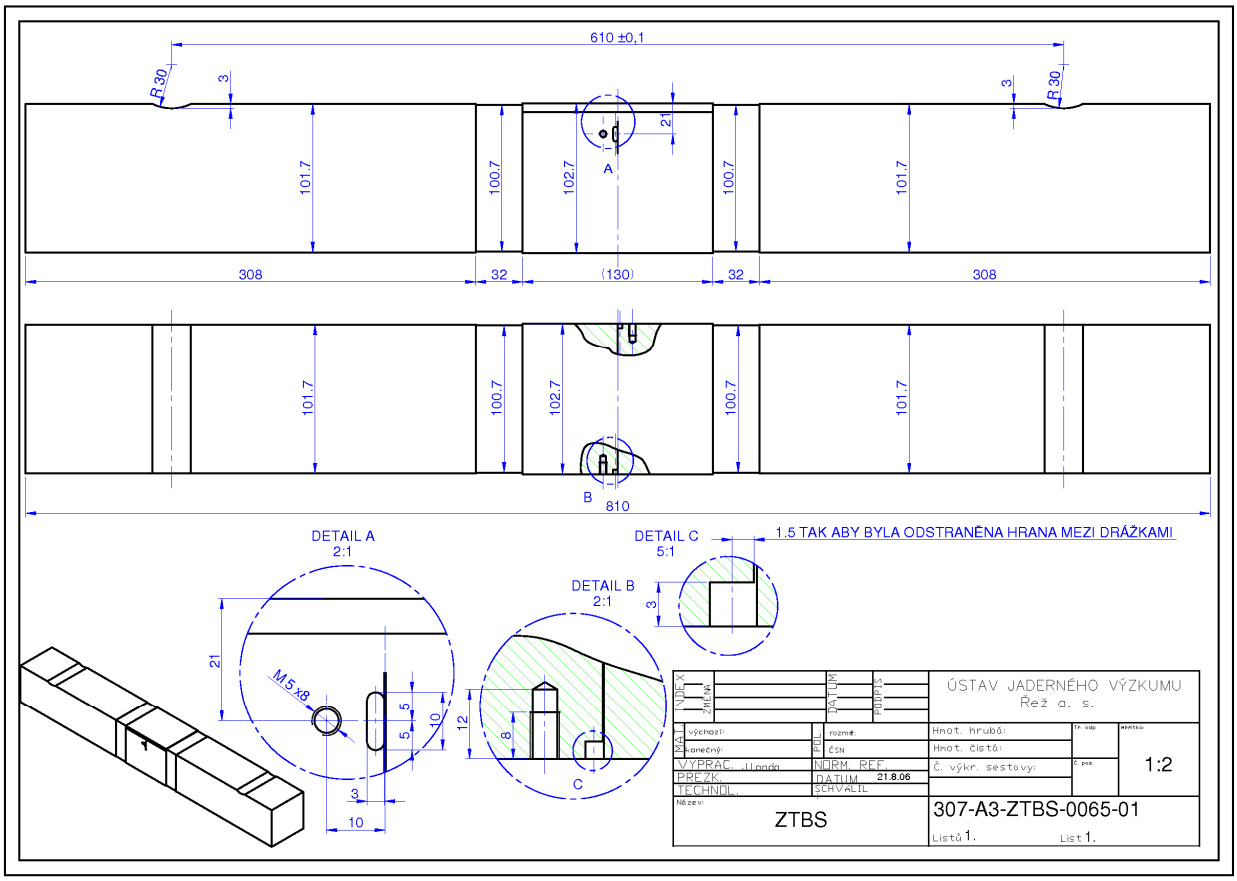

Figure 3 Engineering drawing of the specimens.

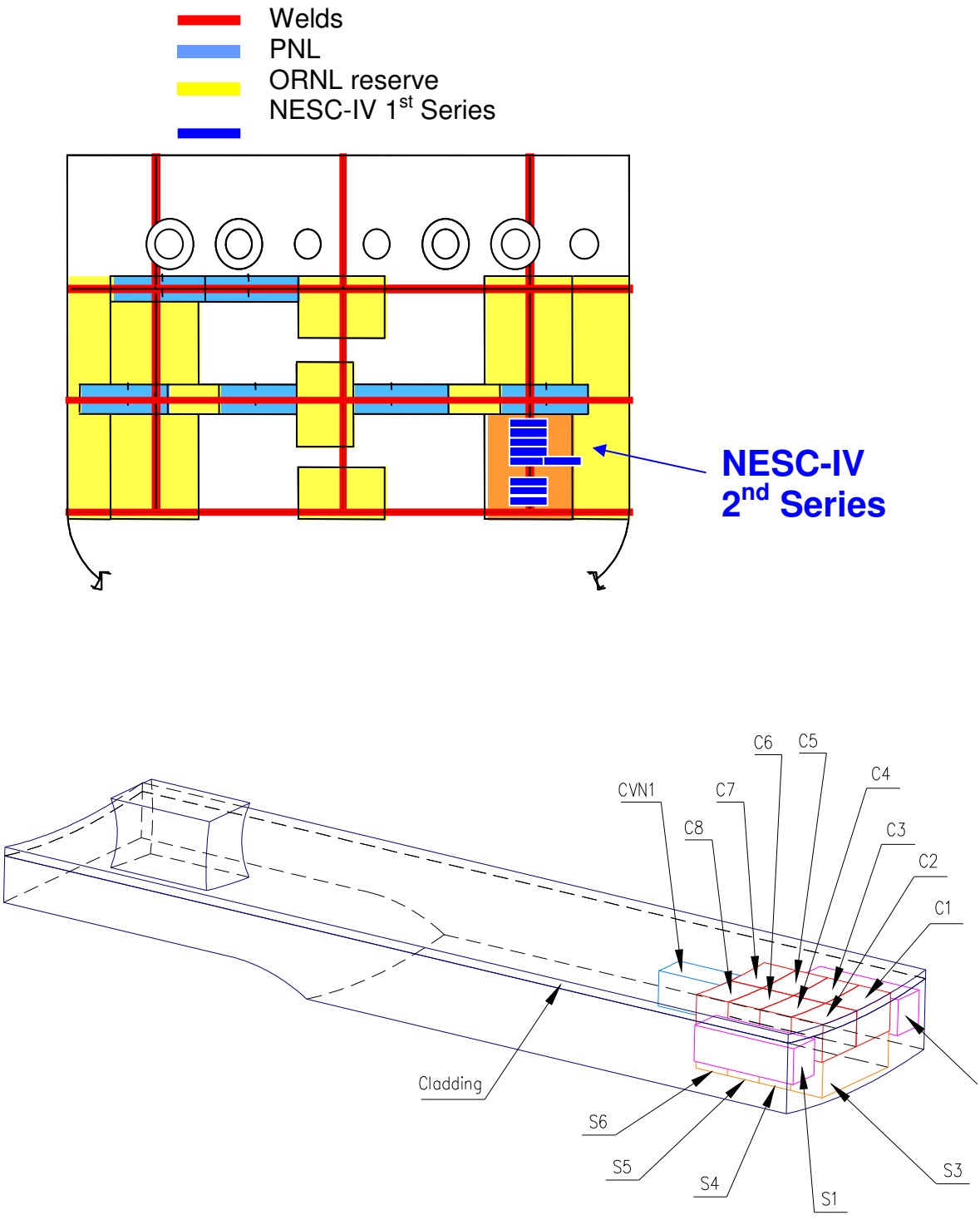

Figure 4 Location of the test sections in the PVRUF shell segment.

Figure 5 The central section of specimen no. 1 prior to testing.

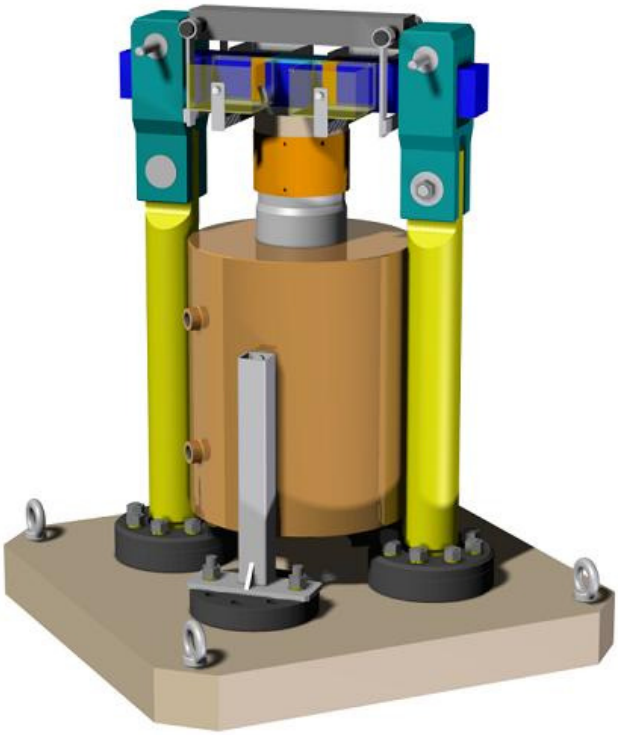

Figure 6 Test rig developed by NRI.

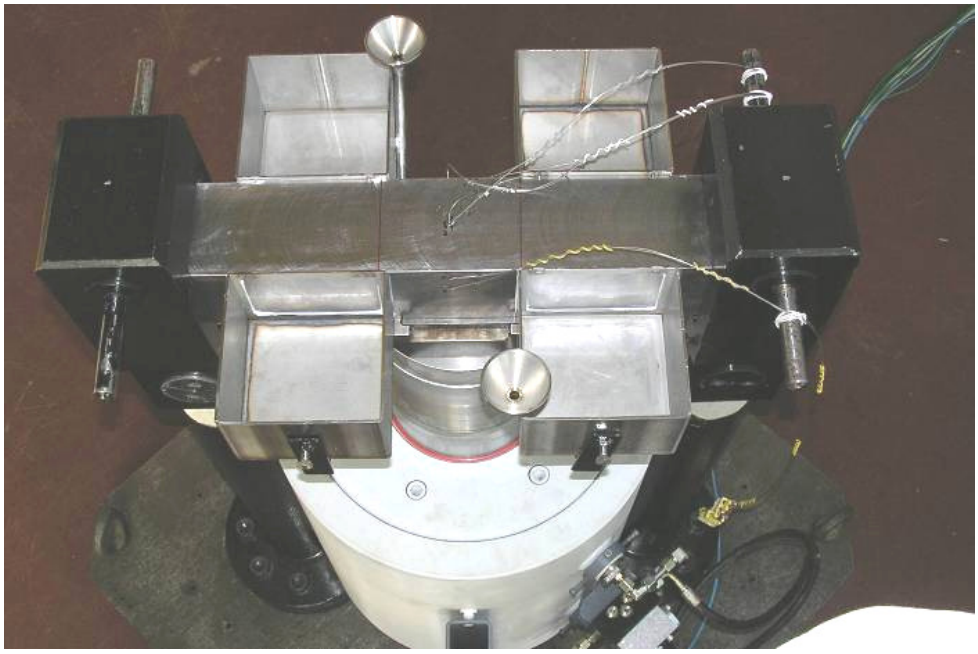

(a)

(b)

Figure 7 System for cooling the test piece: a) the liquid nitrogen baths at either side of the beam; b) addition of liquid nitrogen for the cooling phase.

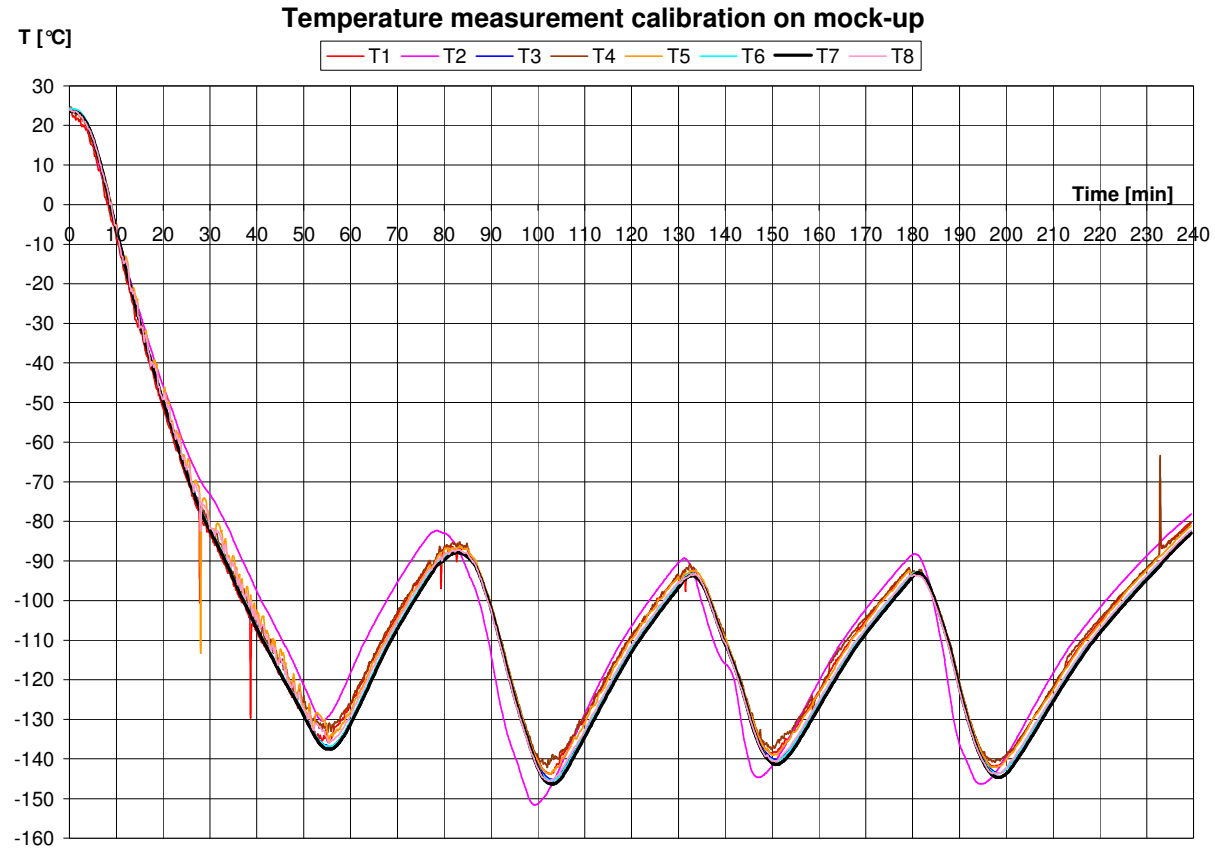

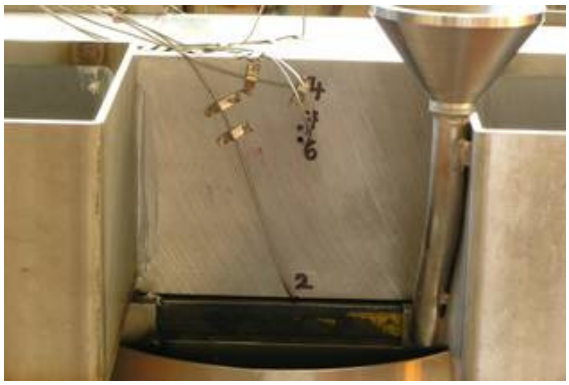

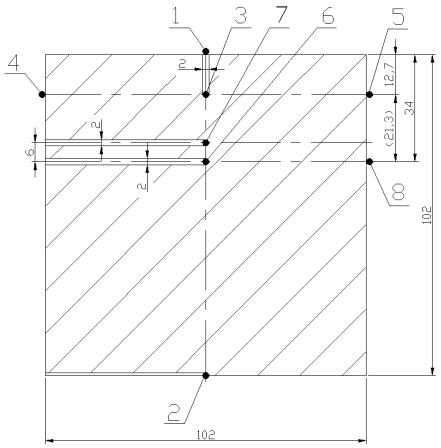

Figure 8 Temperature values recorded during the calibration of the cooling/heating cycle.

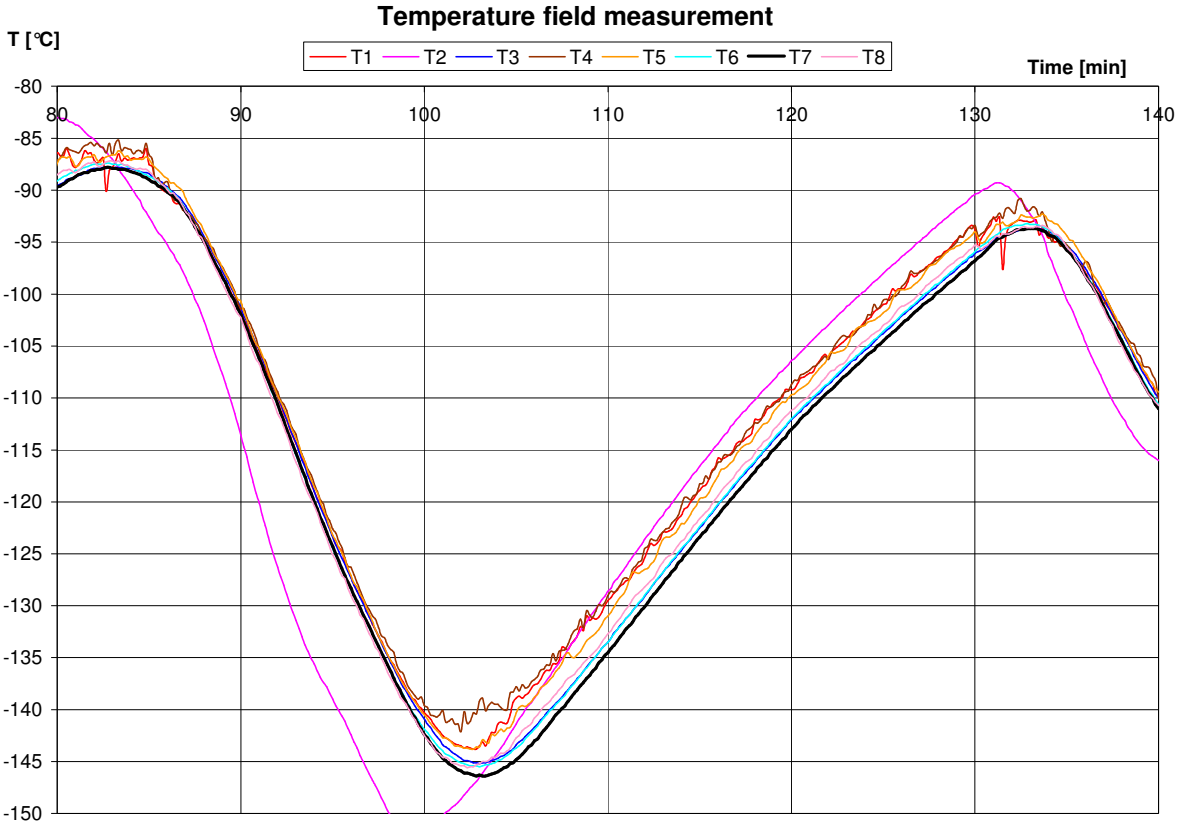

Figure 9 Detail of the 2nd temperature cycle during the calibration. Thermocouple T1 is in the middle of the upper surface; T2 in the middle of the lower surface (in a notch to avoid being squeezed against the support plate); thermocouples T3 - T5 are at the upper crack tip; T6 and T8 are at the lower crack tip and T7 is in the drilled hole of the "real" specimen.

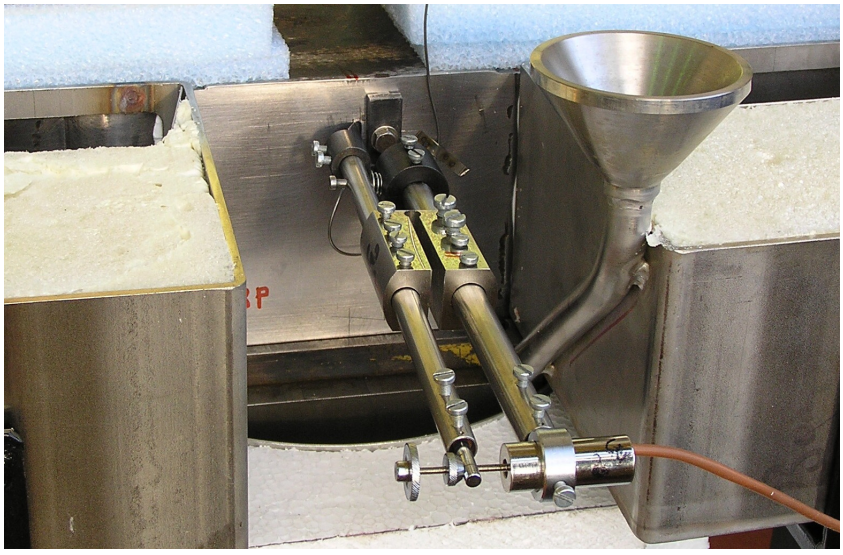

Figure 10 The device for CMOD measurement mounted on the flank of a specimen.

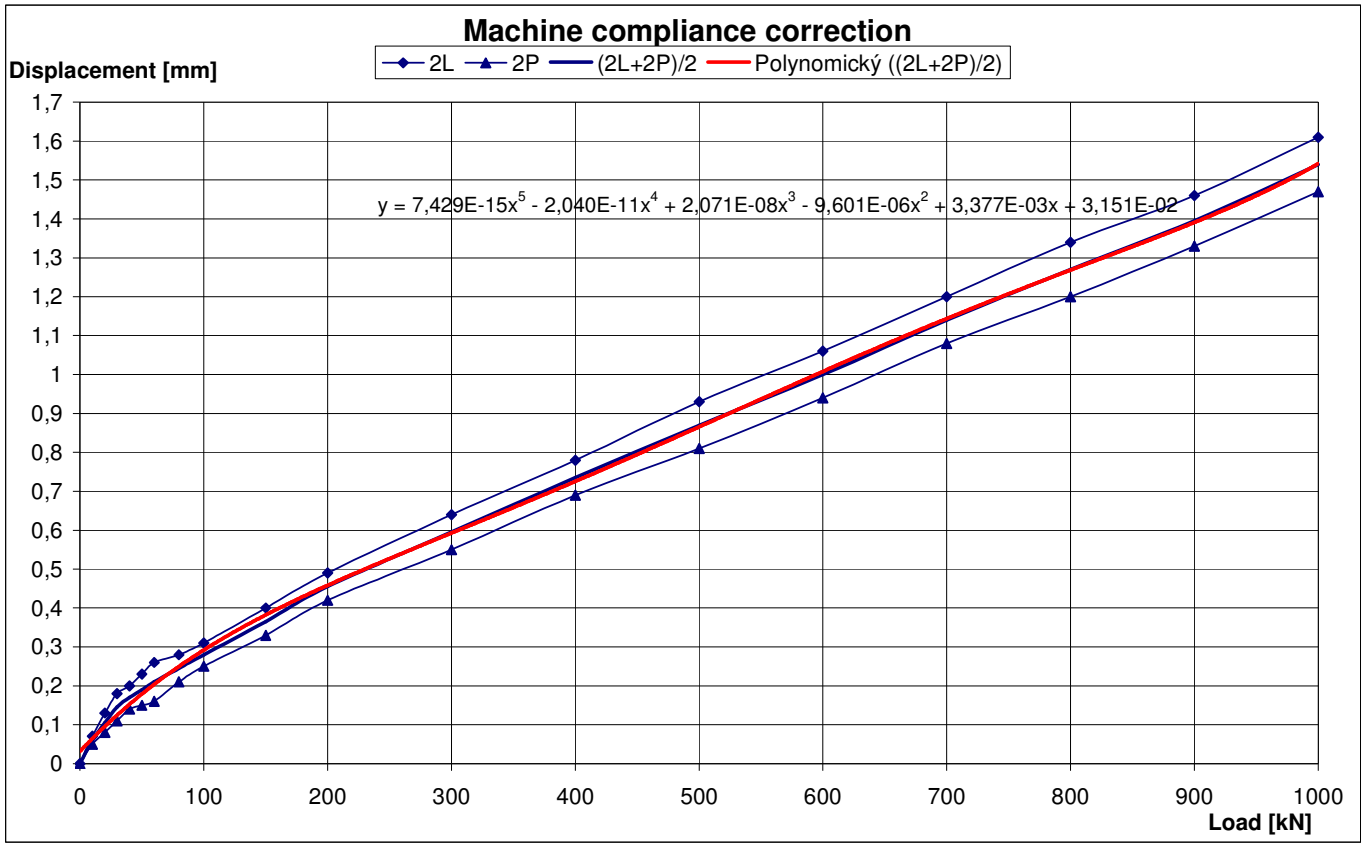

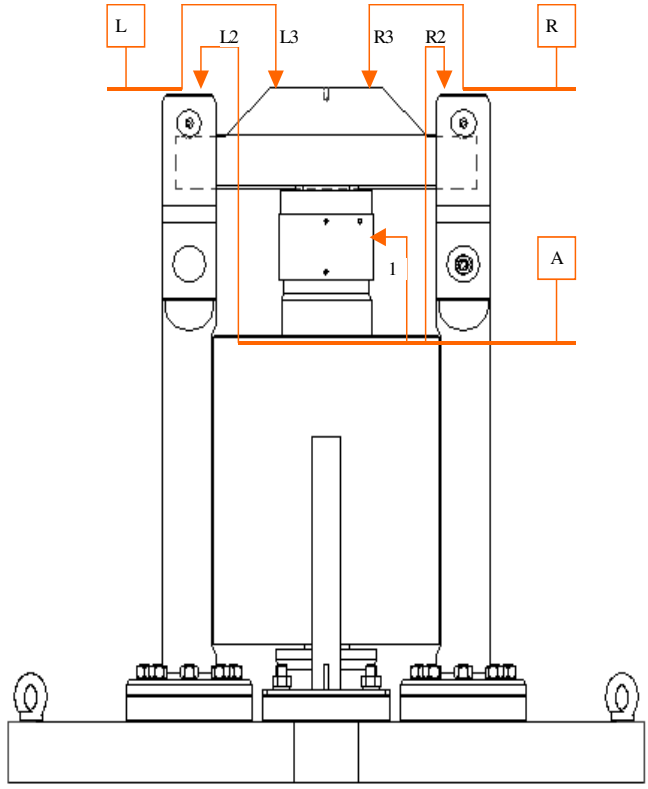

Figure 11 Calibration to establish the compliance correction function for the LLD.

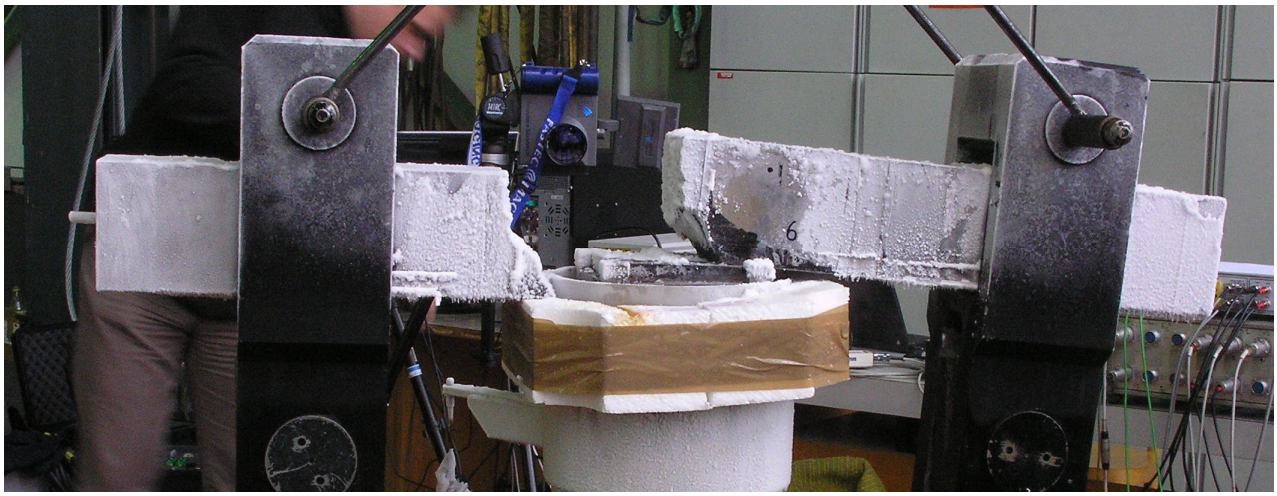

Figure 12 The first attempt to test specimen no. 6 at -110 ^{o}C ended prematurely with failure of the weld between an extension arm and the insert.

Figure 13 Specimen no. 1 after fracture.

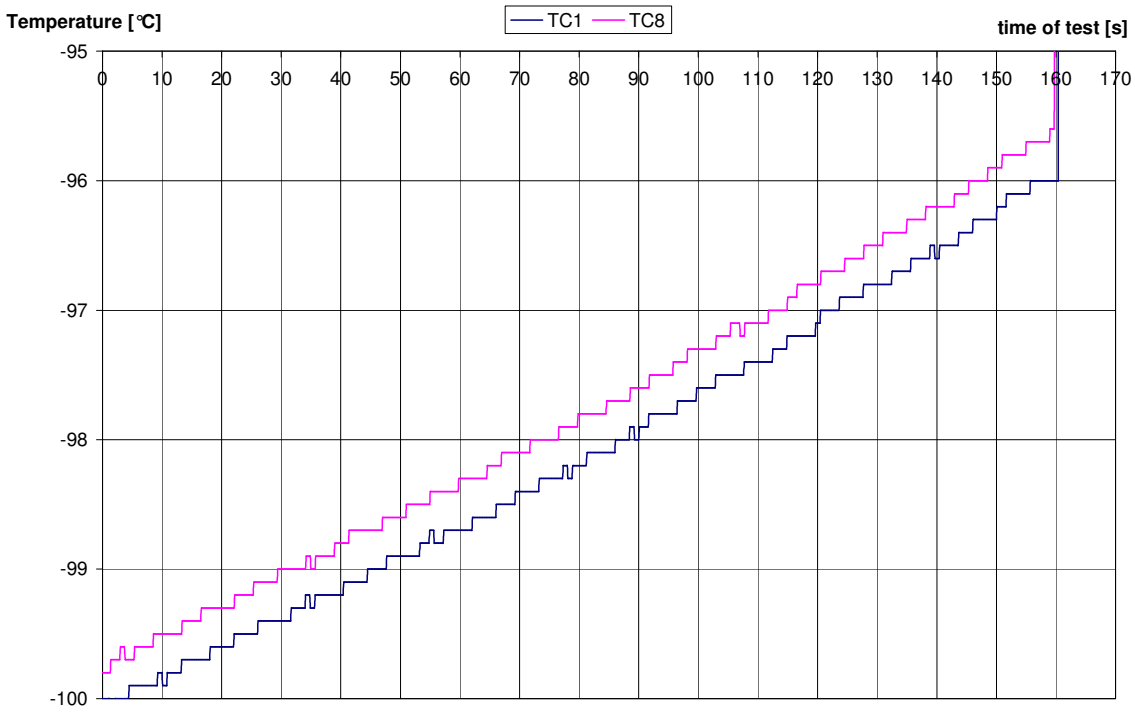

Figure 14 Temperature variation during the test on specimen no. 1 for thermocouple 1 (top centre) and 8 (deep tip on the specimen flank).

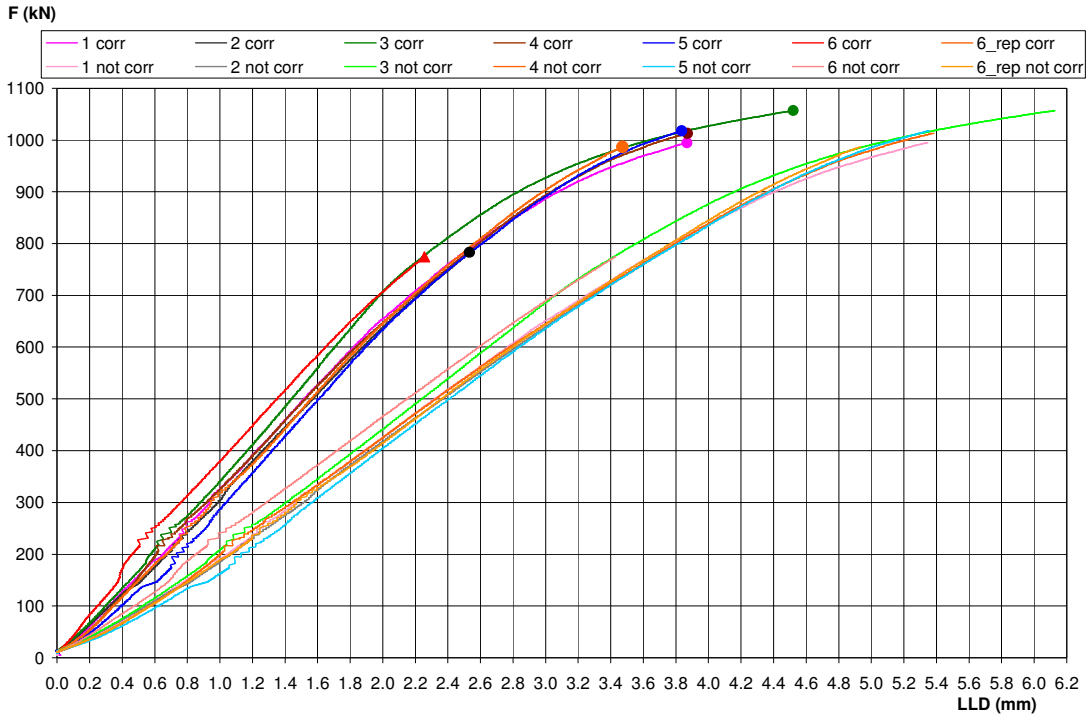

Figure 15 Force as function of load line displacement:
a) "not corrected " values from the piston displacement and
b) "correction" values allowing for the machine compliance.

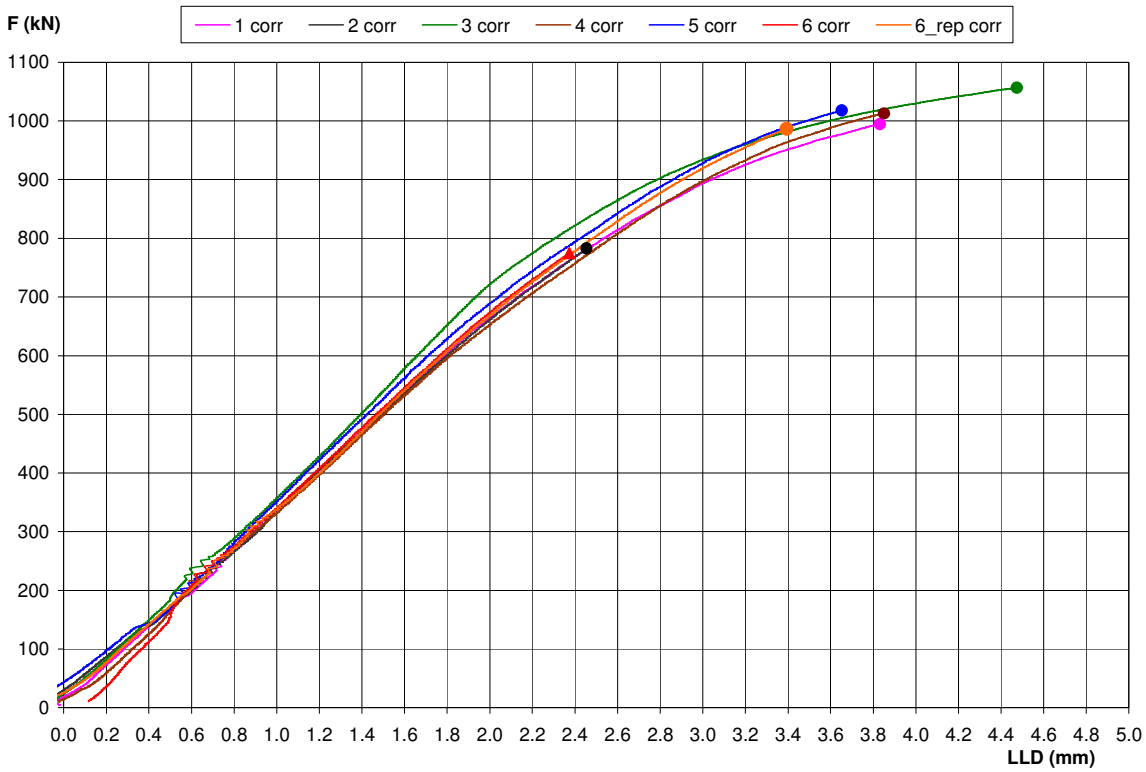

Figure 16 Force as function of load line displacement values adjusted to obtain a common zero point.

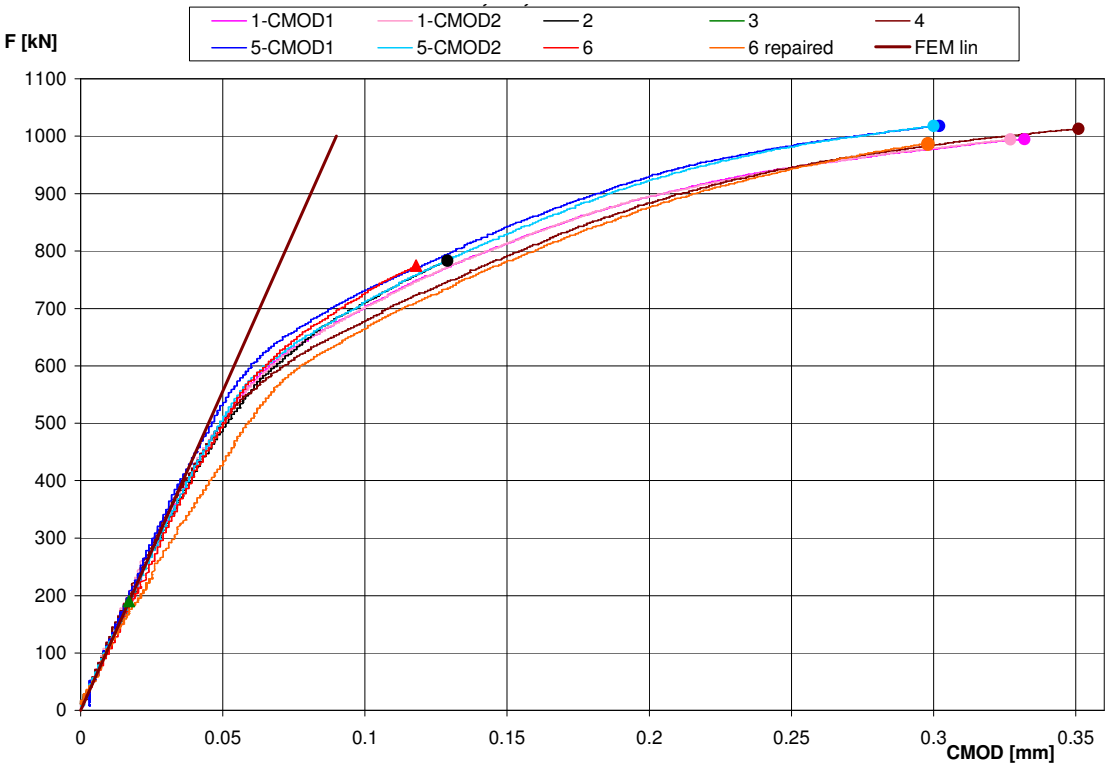

Figure 17 Force as function of crack mouth opening displacement (the black line is from a linear elastic FE calculation of the specimen behaviour).

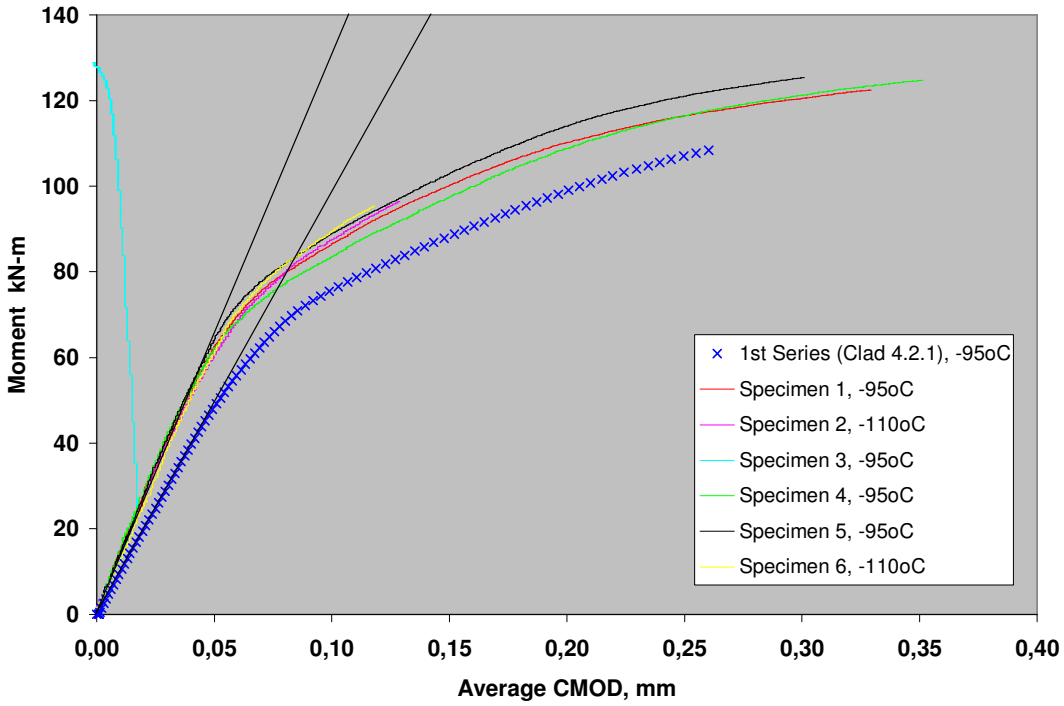

Figure 18 Comparison of the moment vs. CMOD data from the 2nd NRI test series with the NESC-IV Clad 4.2.1 test performed at - 95°C.

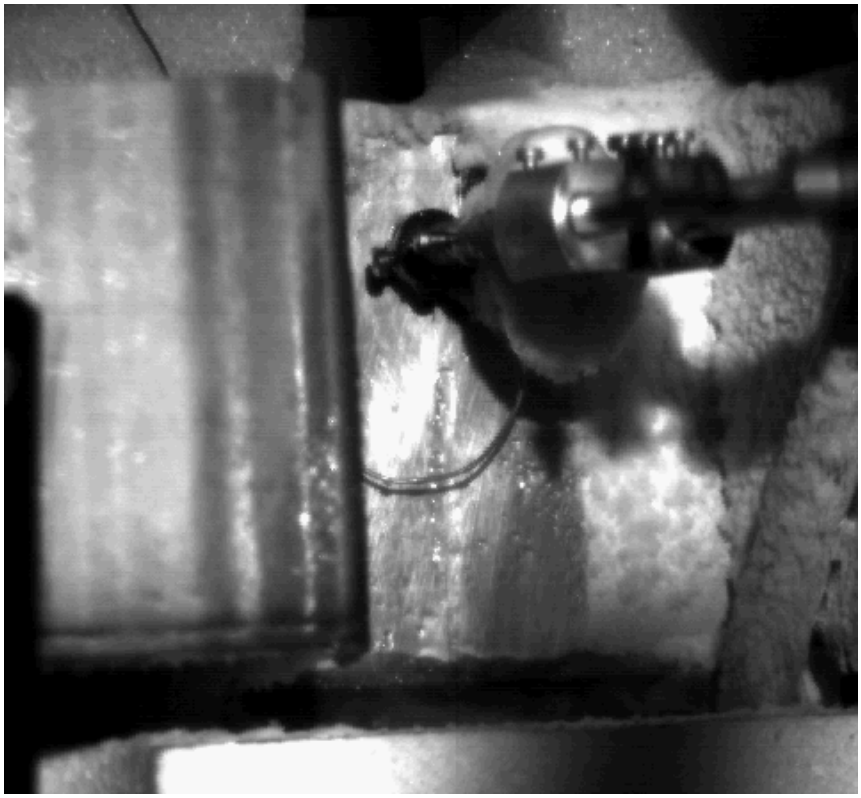

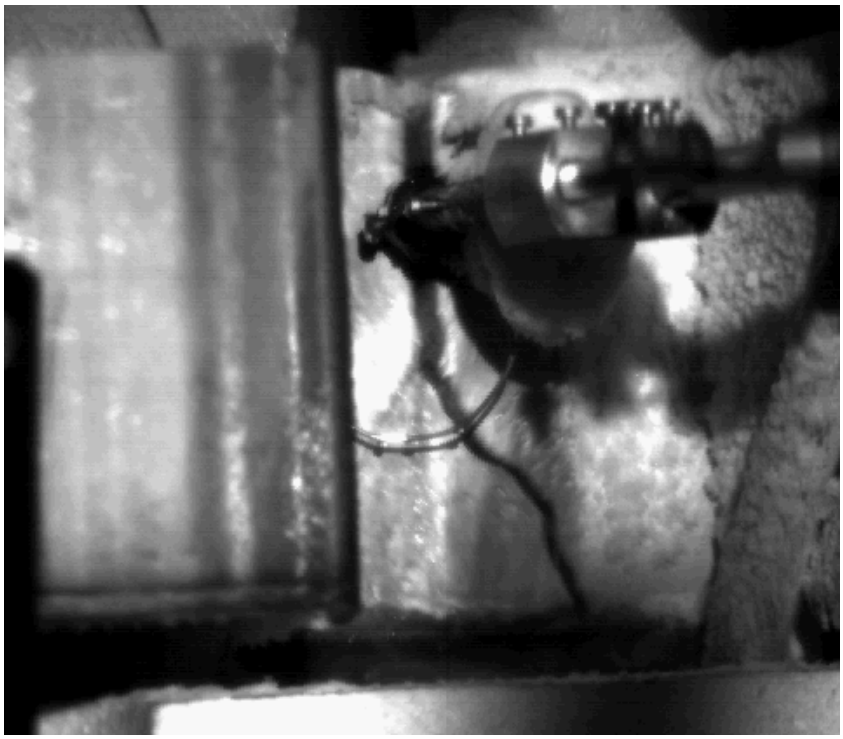

Figure 19 Specimen no. 1 – fracture (recording frequency 1,000 Hz).

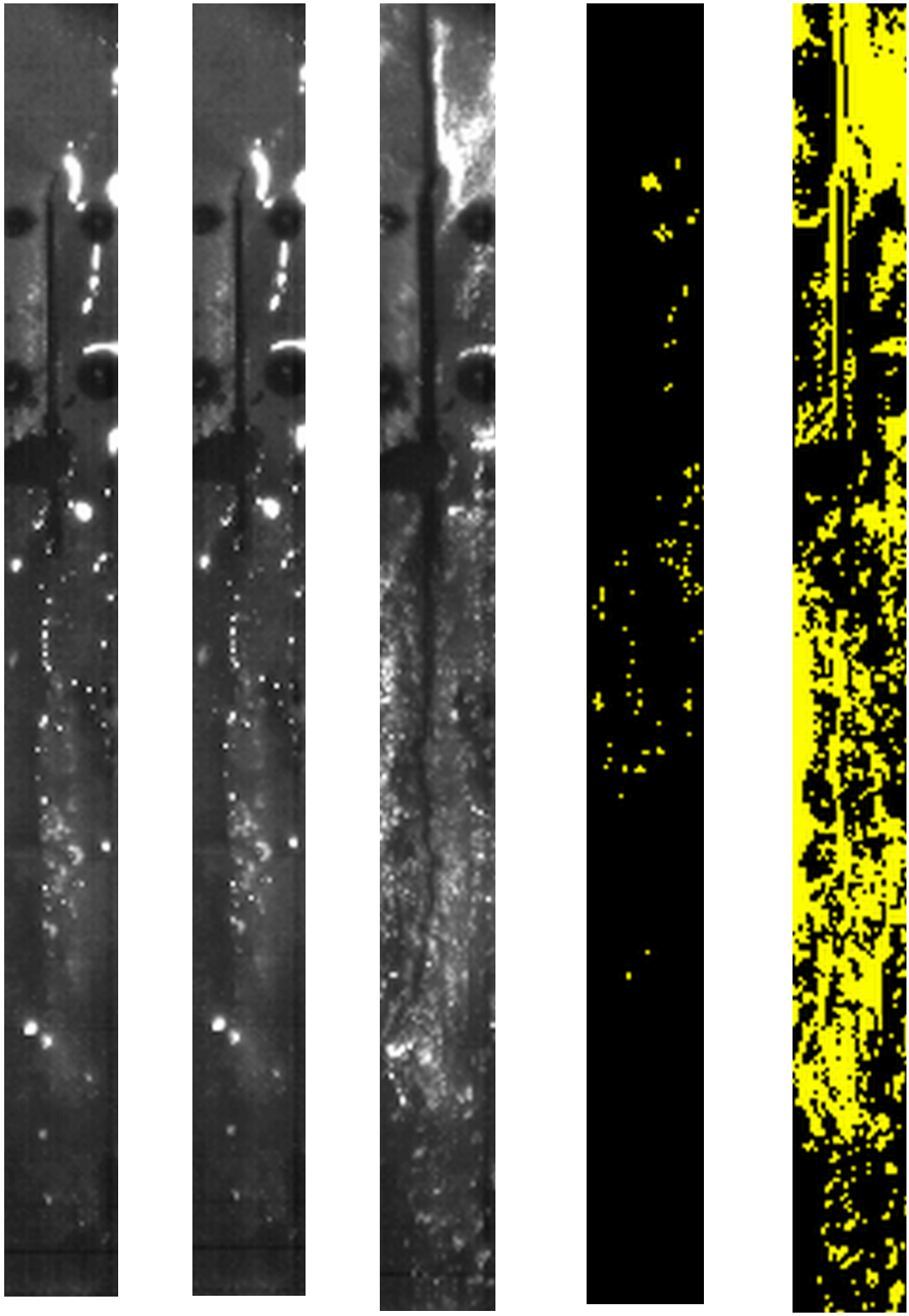

Figure 20 Specimen no. 2 - crack tip video images at 16,000 Hz; the left-hand three images are successive frames at the moment of fracture; the right hand images represent the digital difference between frames 1 & 2 and between 2 & 3 respectively.

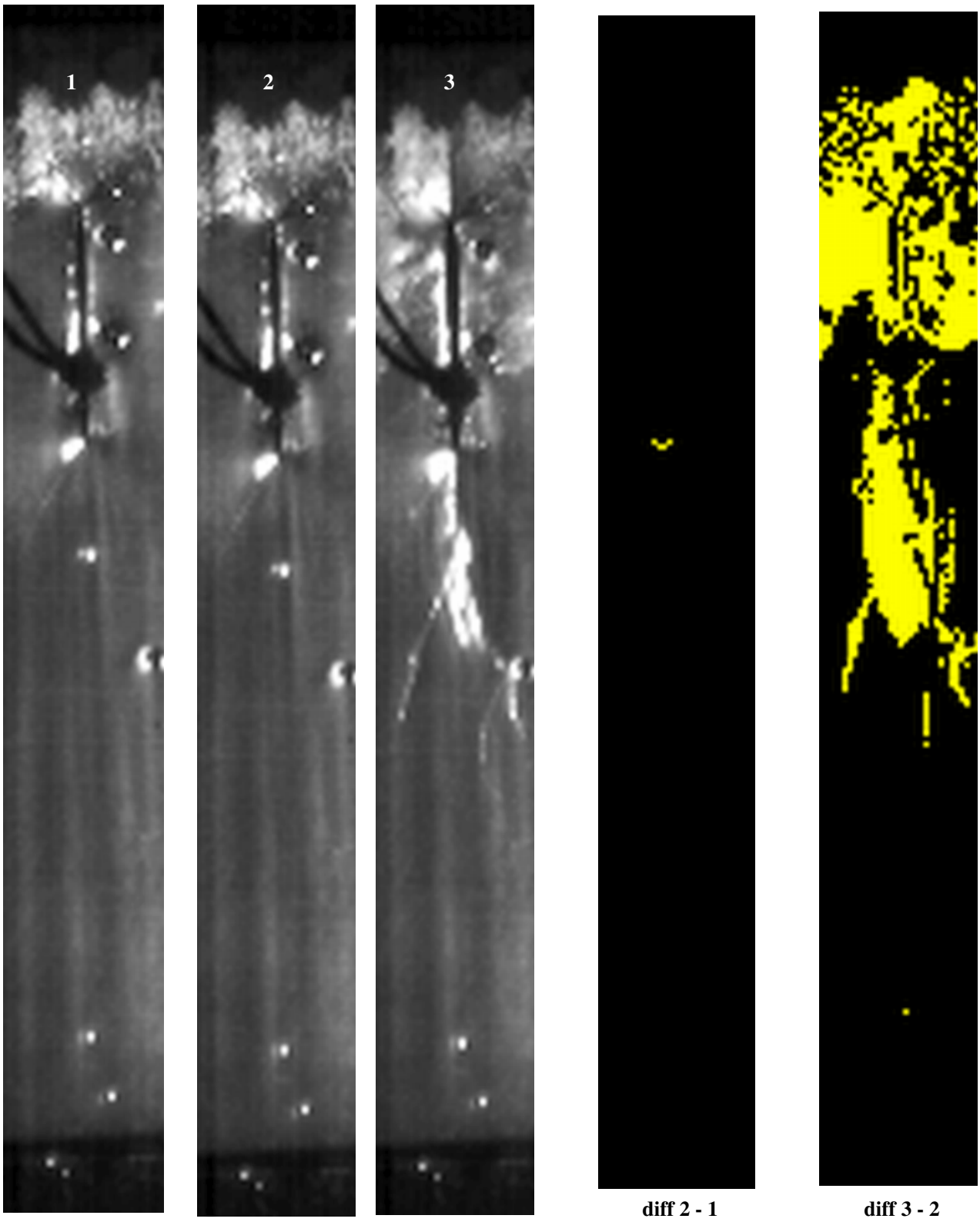

Figure 21 Specimen no. 3 - crack tip video images at 16,000 Hz; the three left-hand images are successive frames at the moment of fracture; the right hand images show the digital difference between frames 1 & 2 and between 2 & 3 respectively.

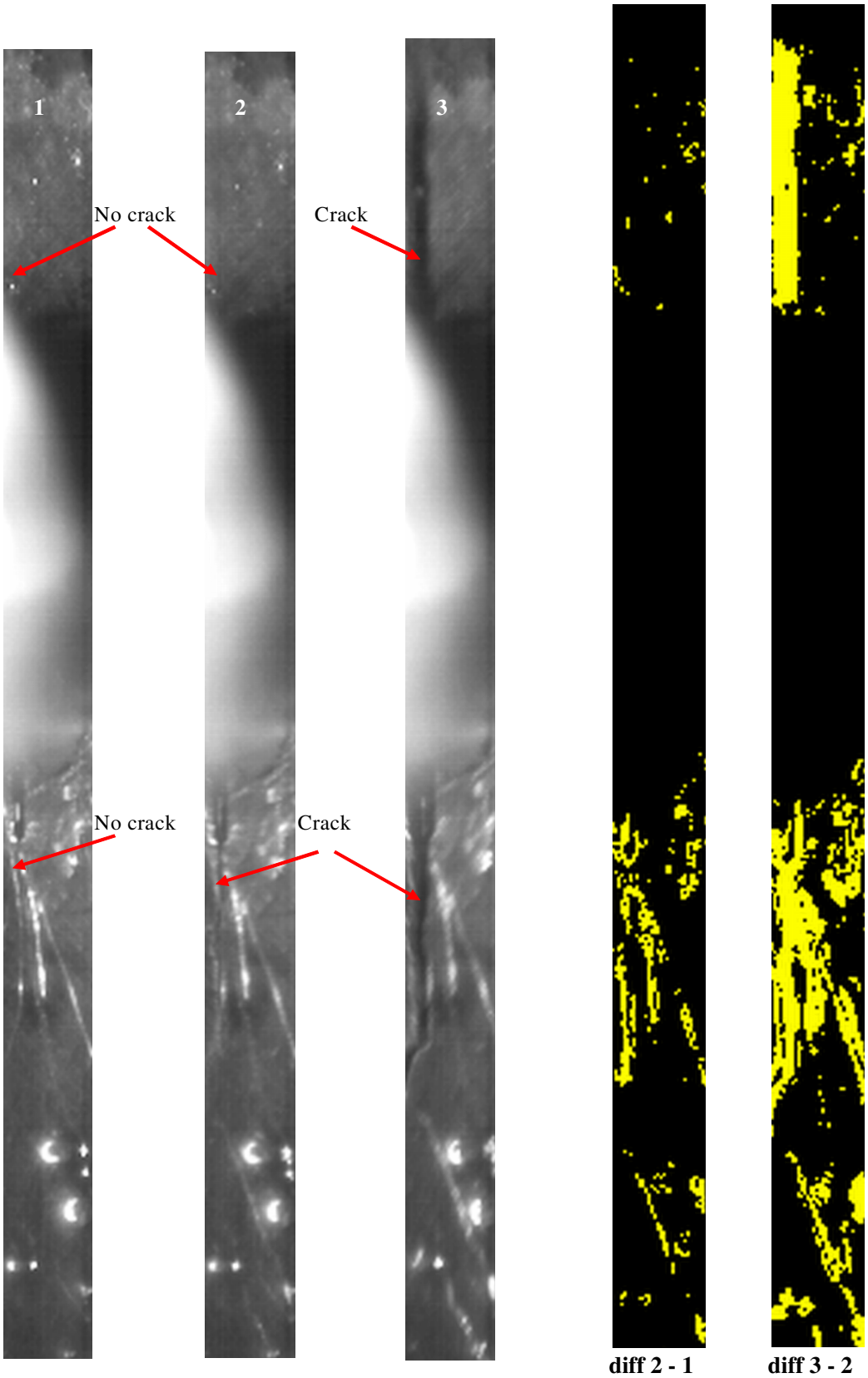

Figure 22 Specimen no. 5 - crack tip video images at 16,000 Hz; the left-hand three images are successive frames at the moment of fracture; the right hand images represent the digital difference between frames 1 & 2 and between 2 & 3 respectively.

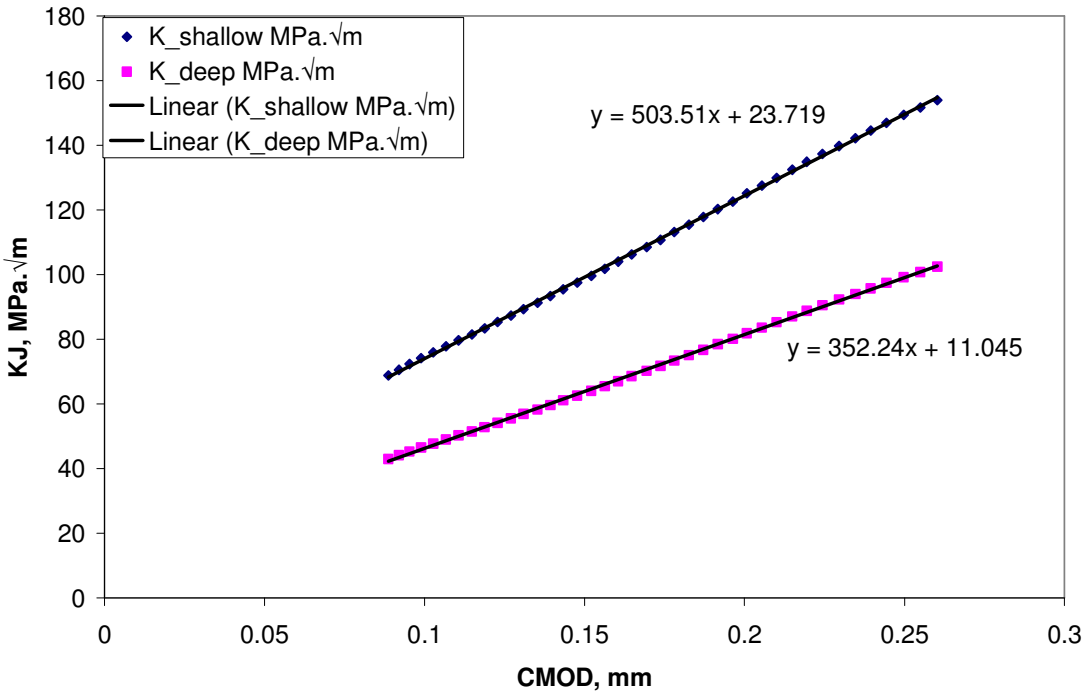

Figure 23 The K_J vs. CMOD relationships for the shallow and deep crack tips established from elastic-plastic FE simulations in the NESC-IV project.

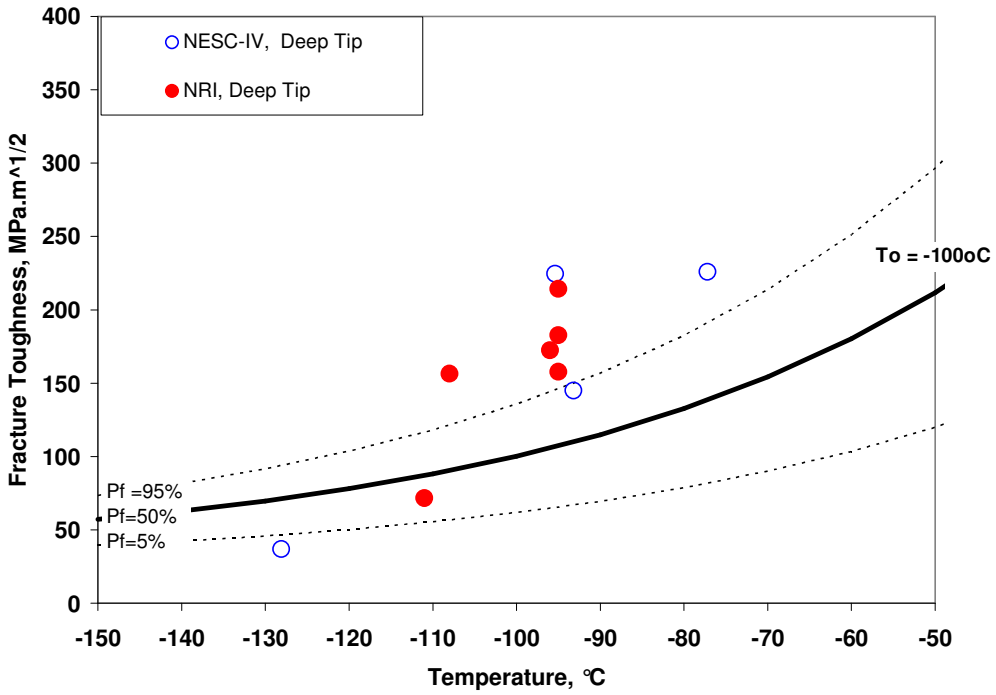

Figure 24 The Master Curve with T_o = - 100 ^oC with experimental deep tip data for the PVRUF shell.

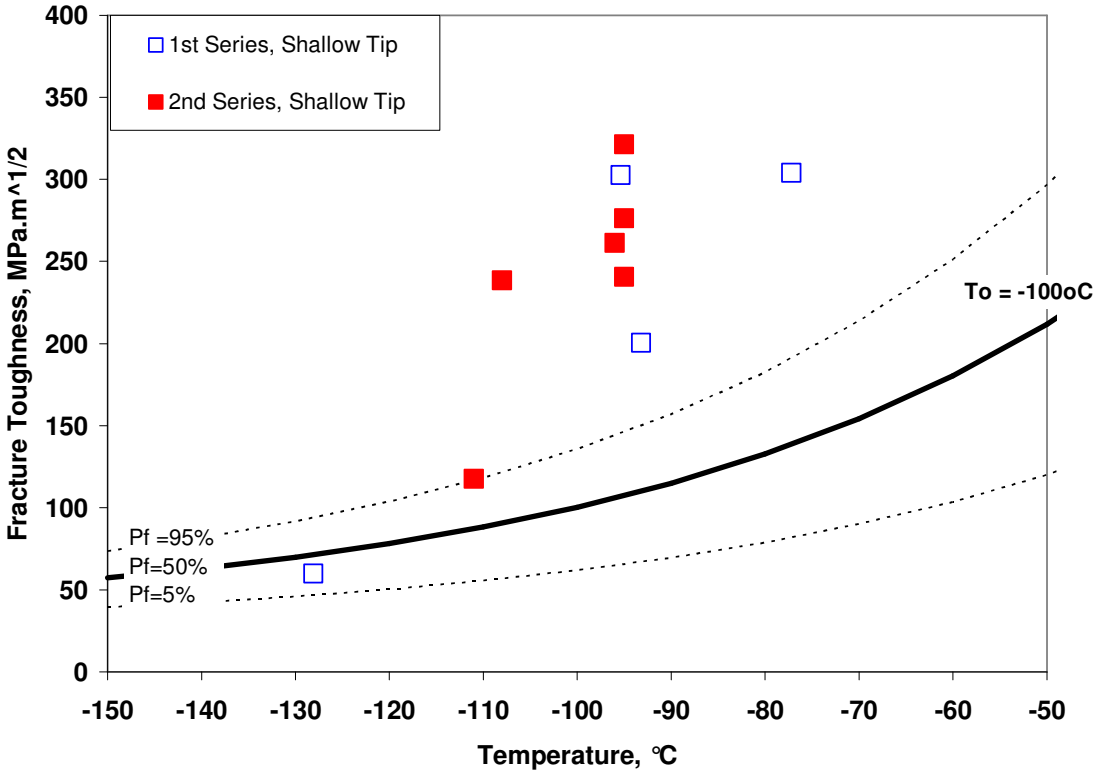

Figure 25 Master Curve plots showing the present NRI data with data points from the NESC-IV test series for the shallow tip.

European Commission

EUR 23970 EN – Joint Research Centre – Institute for Energy
Title: Fracture Tests to Study the Behaviour of Simulated Sub-Surface Flaws in a Reactor Pressure Vessel Steel
Authors: N. Taylor, P. Minnebo, E. Paffumi, J. Palyza, V. Pistora

Luxembourg: Office for Official Publications of the European Communities
2009
EUR – Scientific and Technical Research series

Abstract

The NESC-IV project (2000 - 2005) addressed the transferability of fracture toughness data from laboratory specimens to applications that assess the integrity of reactor pressure vessels. This project included a series of uniaxial bend tests on large beams with a simulated shallow, sub-surface flaw. The results of these experiments pointed towards a significant constraint-loss effect in the ductile-to-brittle transition temperature range of the used steel, but in view of the inherent scatter in fracture toughness of low alloy steels in the given regime, further testing was recommended.

Therefore the scope of present project was to perform a set of six additional tests with nominally identical test piece geometry, material and loading arrangements, so as to obtain a statistically more relevant data set. The Institute for Energy contracted the Nuclear Research Institute in Rez to perform these experiments. Following the successful execution of the tests, a preliminary fracture mechanics analysis was made to compare estimates of the stress intensity values at failure with the material's Master Curve. The results confirmed the constraint-loss effect, which had been observed in the previous NESC-IV test series. Moreover it was found that some aspects needed further attention, such as detailed finite element modelling of the experimental arrangements and accurate characterization of the test material's fracture toughness. The latter should also consider material inhomogeneity issues.

The mission of the JRC is to provide customer-driven scientific and technical support for the conception, development, implementation and monitoring of EU policies. As a service of the European Commission, the JRC functions as a reference centre of science and technology for the Union. Close to the policy-making process, it serves the common interest of the Member States, while being independent of special interests, whether private or national.

JRC
EUROPEAN COMMISSION

Publications Office
Publications.europa.eu